Characterization of Long-Chain Aliphatic Polyesters: Crystalline and Supramolecular Structure of PE22,4 Elucidated by X-ray Scattering and Nuclear Magnetic Resonance

M. G. Menges[†] and J. Penelle[‡]

Department of Polymer Science and Engineering, University of Massachusetts, Amherst, Massachusetts 01003

C. Le Fevere de Ten Hove and A. M. Jonas

Université de Physique et de Chimie des Hauts Polymères, Université Catholique de Louvain, B-1348 Louvain-la-Neuve, Belgium

K. Schmidt-Rohr*

Department of Chemistry, Iowa State University, Ames, Iowa 50011

Received July 17, 2007; Revised Manuscript Received September 9, 2007

ABSTRACT: The crystalline packing and the phase structure of a long-chain aliphatic polyester, $(O(CH_2)_{22}OOCCH_2CH_2CO)_n$, PE22,4, have been studied in molecular detail by small-angle X-ray scattering (SAXS) and wide-angle X-ray diffraction (WAXD) experiments as well as various solid-state nuclear magnetic resonance (NMR) methods, in particular two-dimensional double-quantum spectroscopy (DOQSY) NMR. The volume crystallinity is 73 ± 3% according to quantitative ^{13}C NMR and SAXS analyses. The DOQSY NMR spectra show signal characteristic of trans ester groups incorporated into straight poly(methylene) chains, as expected on the basis of WAXD. DOQSY spectra of singly ^{13}COO-labeled diesters prove close proximity of ester groups in neighboring chains, confirming the ester layering deduced from SAXS, with three diester layers per crystallite. SAXS shows a 37° chain tilt with respect to the diester layers and crystallite surface, and the DOQSY NMR spectra confirm the resulting significant displacement of ester groups along neighboring chains. The data suggest a $\alpha\beta_{22}$ tilting of the chain axes. NMR detects no significant disorder along the chain axes; this suggests that the disappearance of (h, k, $l \neq 0$) reflections in WAXD is due to the small crystallite thickness, which is 5.6 ± 0.5 nm according to SAXS. The DOQSY NMR patterns show that the planes of the chains are far from the perpendicular relative orientation found in orthorhombic polyethylene, constraining the angle between the (normals to the) O−C═O ester planes to 55° ± 20°. DOQSY NMR also indicates that ∼1/3 of the COO groups directly at the crystalline−amorphous interface are disordered. The chain loops in the amorphous phase contain only 6% of the esters and thus mostly consist of the C_{22} polymethylene section of one C_{26} repeat unit. The C_{22} loops connect ∼71% of the ends of crystalline stems, while 9% are terminated by chain ends and 20% are connected to a loose loop or tie molecule. NMR relaxation measurements confirm that, in spite of the relatively small fraction of ester groups among the poly(methylene) chains, they strongly suppress the fast 180° chain flips observed in polyethylene crystallites.

Introduction

Chain architecture of common commercial semicrystalline polymers such as polyethylene is of importance when considering polymer properties such as crystallinity, strength, and viscoelasticity. For polyolefins, a family of materials with different properties can be tailored through appropriate choice of monomer, amount and nature of comonomer, and polymerization conditions. While high-density polyethylene (HDPE) consists predominantly of a polymethylene backbone with only a low branching content, linear low-density polyethylene (LLDPE) contains branches of a certain amount and given length dictated by comonomer content and nature that are randomly distributed throughout the backbone. These short chain branches act as "structural defects" and are usually rejected from the polyethylene crystal if longer than one carbon unit. Although in recent years more uniform incorporation of comonomer has been achieved through advances in metal catalysis, the distribution of the distance between comonomer units is still statistical. This prevents those polyolefins from being useful as model polymers for studying relations between chemical architecture, crystalline microstructure, and chain dynamics in detail.

While polyethylene copolymers allow only limited control over polymer crystallization and morphology through van der Waals and steric forces, polypeptides and polyamides have excellent control due to interchain hydrogen bonding.[1] Whether such a degree of control over polymer morphology can be attained through weaker van der Waals forces remains an open issue. To tackle this question, a valid model system will consist of an aliphatic backbone mimicking polyethylene and contain "structural defects" at controlled distances. The "structural defects" will then, like the short-chain branches in LLDPE, affect the lamellar thickness, crystallinity, chain dynamics, and ultimately strength. Out of the variety of defects imaginable, we have chosen ester groups. The PE-like polyesters can be synthesized through polycondensation of long-chain diols and

* Corresponding author. E-mail: srohr@iastate.edu.
[†] Present address: Institut für Mikrotechnik Mainz GmbH, Carl-Zeiss-Strasse 18-20, 55129 Mainz.
[‡] Present address: Institut de Chimie et des Matériaux Paris-Est, 2-8, rue Henri Dunant, 94320 Thiais, France.

10.1021/ma071590p CCC: $37.00
Published on Web 11/06/2007

short-chain diacids. Those will yield a polyethylene-like backbone, whose length is determined by the length of the diol, and a relatively small defect that can potentially be varied to yield branched or charged systems. Through variation of diol length, the defect concentration can be varied while still maintaining polyethylene-like character.

We have previously reported on the morphology of such branched model polymers[2] and on the synthesis and general characterization of linear analogues.[3] In this paper, we report in much more detail on the chain conformation, packing, and phase structure in the crystallites of one such linear polyester (PE22,4) by state-of-the-art solid-state NMR experiments and detailed X-ray diffraction studies. The structural NMR investigations are based mainly on the double-quantum spectroscopy (DOQSY) experiment, which has been used previously to study chain conformations and packing in amorphous polymers.[4] DOQSY NMR measures the relative orientation of pairs of ^{13}C-labeled segments that are close in space by correlating their chemical shift anisotropies. This allows us to distinguish all-trans conformations and other structures. If ^{13}COO groups on neighboring chains are sufficiently close in space, chain packing can be characterized with high angular resolution. The coherence transfer between the ^{13}C spins is modulated by the distance- and orientation-dependent $^{13}C-^{13}C$ dipolar coupling, which provides additional structural information. On the basis of the NMR and scattering data, chain folding statistics can be analyzed and a detailed model of the polymer packing on the 5 nm scale has been constructed.

In order to gain insight into the influence of ester group placement along the backbone on chain mobility, NMR relaxation times $T_{1\rho}$ and $T_{1,C}$ were measured in PE22,4. We explore to what extent the ester groups slow down the chain flips in the crystallites compared to polyethylene; these dynamics have important effects on creep as well as ultradrawability.[5−7] As an additional comparison, relaxation times were also measured for PE(32/12),4, a structural isomer of PE22,4 but with slightly randomized placement of ester groups through incorporation of both 1,12-dodecanediol and 1,32-dotriacontanediol in the polyesterification, which results in a disruption of close ester packing.

Experimental Section

Materials. Unlabeled succinic acid was obtained from Aldrich and used without further purification. ^{13}C-labeled potassium cyanide was obtained from Cambridge Isotope Laboratories and used as received. 1,12-Dodecanediol was obtained from commercial sources. Reagents used in the synthesis of 1,22-docosanediol, 1,32-dotriacontanediol, and labeled succinic acid were obtained from commercial sources and used as received. Where necessary, solvents were dried using standard procedures. Prior to polymerization, monomers as well as *p*-toluenesulfonic acid catalyst were dried under vacuum overnight.

Monomer Synthesis. 1,22-Docosanediol was synthesized in three steps using a modified literature procedure starting from commercially available 11-bromoundecanol.[8] The hydroxyl functionality was protected with trimethylsilyl chloride followed by exchange of the bromide with iodide via the Finkelstein reaction to increase the reactivity in the subsequent Wurtz coupling performed under sonication. After acidic workup, the 1,22-docosanediol is obtained in an overall yield of 50%. 1,32-Triacontanediol was synthesized in five steps using a procedure developed by Hünig and Buysch from 1-morpholinocyclododecene and sebacoyl chloride.[9] After (2 + 2) cycloaddition of enamine with ketene which is formed in situ from diacid chloride, the resulting tetraketone is ring opened with sodium hydroxide to yield 13,20-dioxo-1,32-triaconatanedioic acid. The ketone functionalities are reduced by Wolff−Kishner reaction utilizing hydrazine. The formed diacid is then esterified to facilitate reduction of carboxyl functionalities to alcohols via $LiAlH_4$. 1,32-Dotriacontanediol is obtained in an overall yield of 36%.

The ^1H and ^{13}C NMR spectra of 1,22-docosanediol and 1,32-dotriacontanediol were fully compatible with the expected structure, and after purification no side product was detected. The infrared spectra showed Davydov splittings for the peaks at 1420/1430 and 720/730 cm^{-1}, which is typically observed for monoclinically or orthorhombically packed *n*-paraffins. 1,22-Docosanediol and 1,32-dotriacontanediol both show a reversible solid−solid phase transition attributed to a rotator phase transition as has previously been observed for long-chain diols.[10] Melting endotherms are observed at 105 and 111 °C, respectively.

Singly and doubly ^{13}COO-labeled succinic acid were synthesized through nucleophilic substitution of 3-bromoproprionitrile and 1,2-dibromoethane, respectively, with ^{13}C-labeled potassium cyanide, followed by hydrolysis of the formed dinitriles under basic conditions.[11,12] The resulting diacids were characterized by ^1H and ^{13}C NMR spectroscopy and showed only expected peaks.

Polymer Synthesis. The polyesters were synthesized by melt polycondensation of equimolar amounts of diol and the labeled and unlabeled diacids at 120 °C. After 15 h under atmospheric pressure, vacuum was applied for an additional 15 h to remove water formed during the reaction and drive the polymerization to completion. After cooling to room temperature, the polyesters were dissolved in chloroform, precipitated into methanol, and dried in vacuum. Characterization of the polymers by ^1H and ^{13}C NMR showed only expected peaks with no detectable end-group peaks from methylene groups adjacent to unreacted hydroxyl or carboxylic acid functionalities. PE22,4 decomposes at 327 °C and shows a melting endotherm at 92 °C with an enthalpy of melting of 104 J/g. PE(32/12),4 decomposes at 242 °C and shows a melting endotherm at 87 °C with an enthalpy of melting of 104 J/g. In the IR spectrum, Davydov splitting of the peaks at 1430/1420 and 730/720 cm^{-1} can be observed, again indicative of monoclinic or orthorhombic polyethylene-like crystal packing. The powder WAXD patterns show diffraction peaks similar to those observed for HDPE. GPC analysis of the unlabeled PE22,4 showed a M_w of 14 100 with a polydispersity index of 1.94, while unlabeled PE(32/12),4 possesses a M_w of 7300 and a polydispersity index of 1.86.

Instrumentation and SAXS Data Processing. In the Wurtz coupling reaction, a VCX 600 ultrasonicator with amplitude of 30% was used. Solution ^1H and ^{13}C NMR spectra of the monomers and polymers were obtained in deuterated chloroform at room temperature on a Bruker DPX 300 MHz NMR spectrometer. Infrared spectra were recorded on a Bio-Rad FTS 175C spectrometer using 16 scans. Thermogravimetric analysis was performed on the polymers using a TA Instruments TGA 2950 purged with nitrogen at a scan rate of 10 K/min. The decomposition temperature is reported as 2% weight loss. Melting points were determined using a Perkin-Elmer Pyris DSC purged with helium. The melting points are reported as the onset of the melting endotherm during the second heating run. Indium and eicosane were used for temperature scale calibration, while the enthalpy scale was calibrated with indium. Powder WAXD diffraction patterns were recorded with a Ni-filtered Cu Kα radiation source (wavelength 1.54 Å) and evacuated Statton camera. SAXS measurements used an evacuated Kratky camera (Anton-Paar KKK) with a Braun OED 50 M proportional position-sensitive detector and Ni-filtered Cu Kα radiation (40 kV/300 mA). The data were smoothed and then desmeared using a variant of Glatter's algorithm. Furthermore, parasitic scattering and background were subtracted, and the Lorentz correction was applied. They are reported vs $s = 2\sin(\theta)/\lambda$, where λ is the wavelength and θ half the scattering angle. Fourier transformation of the Lorentz-corrected data $s^2I(s)$ was applied to obtain normalized one-dimensional correlation functions, $\gamma_1(r)$. Molecular weights and distributions were determined by GPC relative to polystyrene standards using a system equipped with Polymer Laboratories PL gel columns, a Polymer Laboratories LC 1120 HPLC pump with

THF as the mobile phase, and an IBM LC9563 variable UV detector set at 254 nm.

Solid-State NMR Parameters. Solid-state NMR experiments were conducted using either a Bruker DSX-300 or a Bruker DSX-400 spectrometer with a magnetic field of 7 or 9.4 T, respectively. Spectra were measured under both static and magic angle spinning (MAS) conditions at ambient temperature. For all MAS experiments, 4 mm diameter zirconia rotors with Kel-F caps were used to hold the samples. The measurements on the Bruker DSX-300 spectrometer used a 5 kHz spinning speed and decoupling with two-pulse phase modulation (TPPM) at $\gamma B_1/2\pi = 63$ kHz.[13] Measurements on the Bruker DSX-400 were performed at a spinning speed of 6.5 kHz to avoid overlap of CH_2 peaks with spinning side bands of the ester signals. For cross-polarization (CP) measurements, a ^{1}H 90° pulse length of 4 μs and contact times of 0.5−1 ms were applied.

For the direct-polarization (DP) experiments to determine the crystallinity, ^{13}C magnetization was excited by a single 90° pulse. To obtain the fully relaxed polymer signal, a spectrum with a recycle delay of 3000 s and 24 scans was acquired. Signals for the noncrystalline all-trans and amorphous regions were obtained with recycle delays of 1 and 10 s, respectively;[5] 2048 scans were added up. In all MAS experiments, the chemical shift calibration is based on a chemical shift of 32.8 ppm for crystalline HDPE.

Spin-diffusion measurements after T_2 filtering, using the Goldman−Shen pulse sequence,[14] were carried out with ^{13}C detection. Lee−Goldburg cross-polarization (LG-CP) of 0.5 ms duration was used to prevent spin diffusion during CP. The crystalline signal will vanish after the dephasing time of ca. 15 μs, whereas most of the amorphous signal is retained and can undergo spin diffusion to the crystallites.

In the static measurements (without MAS, at 298 K), the sample was inserted as a cylindrical block of 4 mm diameter wrapped in Teflon tape into the 4.5 mm coil of a stationary Bruker double-resonance probe. The ^{1}H− and ^{13}C 90° pulse lengths ranged from 2.8−4.1 to 2.4−3.2 μs, respectively. Cross-polarization times ranged from 1 ms for mL-PE22,4 to 1.6 ms for the 100% dl-PE22,4. For the doubly labeled polyesters, a recycle delay of 3 s, an acquisition time of 3.12 ms, and a dwell time of 3 μs were used. For the singly ^{13}COO-labeled polyester, a recycle delay of 2.5 s and an acquisition time of 1.78 ms were used. Within recycle delays of >1 s, spin diffusion equilibrates the magnetization across all of the nanometer-scale structure. Therefore, the shape of the spectrum is independent of the recycle delay. The DQ excitation and reconversion delays, $\tau_{DQ} = 0.7$ for the doubly labeled and $\tau_{DQ} = 1$ ms for the singly labeled polyester, each contained two cycles of the *xy*-16 phase sequence, with slightly different pulse spacings.

For the 2D HH/CSA experiment without MAS, LG-CP with a contact time of 200 μs was used. Thirty-two slices with t_1 increments of 2 μs were acquired with 256 scans per slice. To display dipolar modulation, the same experiment was rerun for eight t_1 values with 1440 scans each.

The $T_{1\rho,H}$ relaxation times in the crystallites were measured at various temperatures with a pulse sequence consisting of a variable ^{1}H spin-lock, cross-polarization to ^{13}C, a 10 s phase-cycled *z*-filter to suppress signal from the noncrystalline regions, and ^{1}H-decoupled ^{13}C detection. The cross-polarization time was 0.5 ms. ^{13}C spin−lattice relaxation times, $T_{1,C}$, were measured by the cross-polarization method developed by Torchia.[15] The 90° pulse lengths were 4 μs for both ^{13}C and ^{1}H, and the cross-polarization time was 0.5 ms.

DOQSY NMR. In DOQSY NMR spectroscopy, the orientation-dependent chemical shift frequencies ω_a and ω_b of two ^{13}C spins coupled by a sufficiently strong dipolar interaction (see more details below) are correlated. The original DOQSY spectrum correlates the sum frequency $\omega_a + \omega_b$ of the double-quantum coherence in the first dimension, ω_1, with the individual chemical shift frequencies ω_a and ω_b of the detected magnetization in ω_2. For simplicity of presentation, all spectra shown in this paper have been sheared by 45° along the vertical direction to yield simple correlation patterns $I(\omega_a,\omega_b)$ that are symmetric with respect to the diagonal.[16]

The spectral intensity pattern in the double-quantum spectrum depends sensitively on both the relative orientation of C−O−C chain-axis directions and the relative orientation of the ester planes in neighboring chains. The chain-axis orientations are reflected in the 2D line shape near the ω_{11} (260 ppm, left) edge of the spectrum, since the corresponding principal axis is oriented within 15° from the chain axis. The shape of the ridge pattern at the right, high-intensity end of the spectrum is an excellent indicator of the relative orientation of ester planes, since the ω_{22} and ω_{33} principal values are parallel and perpendicular to the ester planes, respectively. An experimental determination of this tensor orientation is shown below.

Since the generation of the double-quantum coherence is based on excitation and reconversion by the dipolar coupling, the DOQSY spectra are modulated by $\sin^2(^3/_2\omega_{CC}\tau_{DQ})$. Here, ω_{CC} is the ^{13}C−^{13}C dipolar coupling frequency of the observed pair of ^{13}C spins. It depends on the ^{13}C−^{13}C internuclear distance r_{CC} and on the angle θ_{CC} between the ^{13}C−^{13}C internuclear vector and the external field B_0:

$$\omega_{CC} = \pm 2\pi \cdot 3.75 \text{ kHz}/(r_{CC}^3/\text{Å}^3)(3\cos^2\theta_{CC} - 1) \qquad (1)$$

The typical coupling for a given distance is $\pm 2\pi \cdot 3.75$ kHz$/(r_{CC}^3/$Å$^3)$.

For large distances r_{CC} or for θ_{CC} values near 55°, the dipolar coupling is small and the $\sin^2(1.5\omega_{CC}\tau_{DQ})$ modulation suppresses the corresponding spin-pair signal in the DOQSY spectrum. Examples of the resulting minimum in the spectral intensity will be shown below; it is particularly easy to recognize in the diagonal component of the 2D pattern, since the unmodulated powder line shape is well-known. At the overall double-quantum excitation and reconversion time $2\tau_{DQ} = 1.6$ ms used in the experiments, dipolar couplings of $\omega_{CC} = \pm 2\pi \cdot 50$ Hz, corresponding to a distance of ca. 4 Å, generate significant DQ modulation factors (intensity fractions, where the full intensity is unity) of $\sin^2(1.5\omega_{CC}\tau_{DQ}) = 0.14$. This is detectable, in particular, when the signals of clustered ^{13}COO groups in neighboring molecules add up. For directly bonded aliphatic ^{13}C pairs, homonuclear decoupling during signal detection is desirable.[17] However, in the present sample, it was unnecessary since the ^{13}C−^{13}C distances are so large that the dipolar splittings in the ω_2 dimension are negligible compared to the large chemical shift anisotropy of the ester carbons.

DOQSY spectra were simulated in frequency space, by varying the B_0 field orientation in 1° steps in a segment-fixed frame and calculating the ^{13}C−^{13}C dipolar coupling and chemical-shift frequencies as described in ref 4.

Results

X-ray Scattering. The wide-angle X-ray diffractograms (WAXD) of PE22,4 (see Figure 1a) and of PE(32/12),4 (not shown) exhibit sharp and intense reflections indicative of an orthorhombic unit cell with either O⊥ or O′⊥[18] crystal packing.[18−22] The Lorentz-corrected SAXS diffractogram also exhibits several pronounced peaks (see Figure 1b). The sharp smallest-angle peak is assigned to the long period of 77 Å. In addition, intense reflections are seen at larger angles in the SAXS pattern. These are assigned to the layers of high electron density due to the C═O oxygen formed by diesters included into the crystalline regions.[23,24] These (00l) reflections in the SAXS diffractogram correspond to an internal period of 27 Å. This interpretation is confirmed by analysis of correlation functions calculated from the SAXS curve (Figure 1c) and by direct simulation of the small-angle scattered intensity (Figure 1d) from the one-dimensional electron density perpendicular to the lamellar surfaces (see Figure 1e) using numerical Fourier transformation.[25]

^{13}C MAS NMR Spectra. Figure 2 shows the aliphatic region of the ^{13}C CP/MAS NMR spectrum of PE22,4. It is dominated

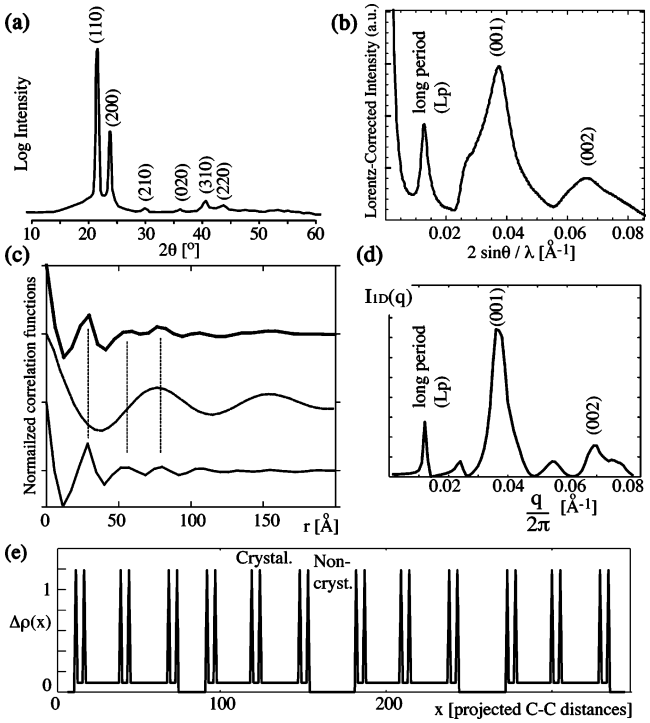

Figure 1. X-ray diffractograms and simulations. (a) WAXD diffractogram of PE22,4. Miller indices (*hkl*) are indicated. (b) Lorentz-corrected SAXS diffractogram of PE22,4. Long period (Lp) and internal-layer (00*l*) reflections are labeled. (c) One-dimensional normalized correlation functions computed from the complete SAXS data (top curve), from the low angle (Lp) peak only (middle curve), or from the (001) and (002) layer lines only (bottom curve). The curves are successively displaced vertically by 1. (d) Simulation of the scattered intensity in (b), obtained as the absolute square of the Fourier transform of a one-dimensional electron-density distribution as shown in (e). (e) Portion of the one-dimensional electron-density distribution (perpendicular to the lamellar surfaces) of the model structure shown in Figure 14. The electron density of the noncrystalline regions has been set to zero. The six "spikes" per crystallite are the C═O oxygens. The crystallinity was 75%, and the variation in the long period was ±5%.

by the crystalline $[-CH_2-]_n$ peak at 32.8 ppm. Nevertheless, significant signal intensity is observed between 30 and 25 ppm, where regular polyethylene shows no distinct bands. In ^{13}C NMR spectra where the signals from the amorphous regions have been suppressed by $T_{1,C}$ filtering of ≥10 s (see Figure 2b), several relatively distinct bands are still observed in this spectral region. These are assigned to methylenes near the ester groups. Clearly, the two OCH_2 groups in each repeat unit are responsible for the peak near 64 ppm. Chemical shift simulations show that the other methylenes within three bonds from an oxygen atom are expected to resonate upfield from 30 ppm. In particular, this includes the methylenes bonded to the ester carbons. Thus, six out of 24 methylenes, or 25% of the methylene signals, are expected to resonate at <30 ppm, which is in good agreement with the spectrum of Figure 2b. The signals of the ester carbons in the ^{13}COO-labeled polymer, shown in Figure 2c, also exhibit a distinct fine structure. A ^1H $T_{1\rho}$-filtered ^{13}COO spectrum, which retains predominantly the signal of the crystalline segments, shows a slight but clear reduction of intensity on the right-hand side of the spectrum (thin line in Figure 2c), which is thus identified as partially noncrystalline. These mobile amorphous components can be selected by a ^1H T_2 filter, as shown below. The static ^{13}C NMR powder spectrum of the ester groups (see Figure 2d) shows no signs of a motionally narrowed component.

The signal of CH_2 groups in the amorphous regions is hardly recognizable in the ^{13}C CP/MAS spectra of Figure 2. However,

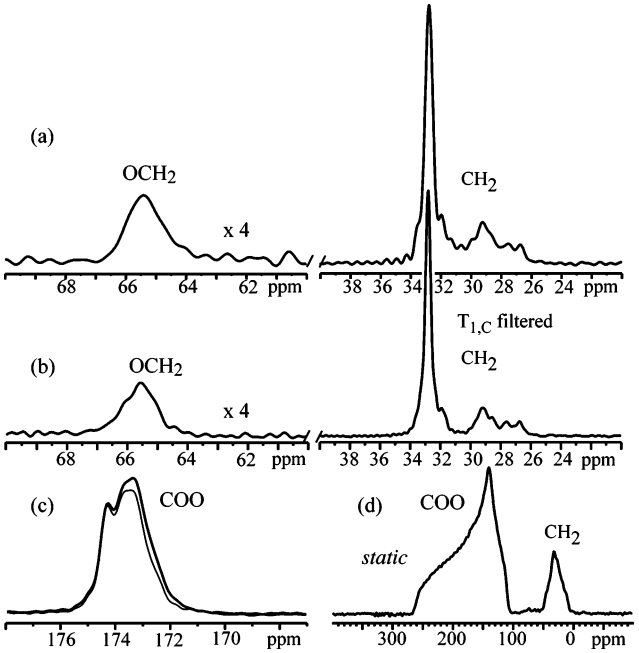

Figure 2. ^{13}C NMR spectra of doubly ^{13}COO-labeled PE22,4. (a) CP/MAS spectrum, CH_2 regions. (b) The same spectral regions after a $T_{1,C}$ filter, which selects rigid segments. (c) COO region of the spectrum of ^{13}COO-labeled PE22,4. Thin line: corresponding ^1H $T_{1\rho}$-filtered spectrum. (d) Static spectrum of ^{13}COO-labeled PE22,4, showing ^{13}COO and $[-CH_2-]_n$ powder patterns.

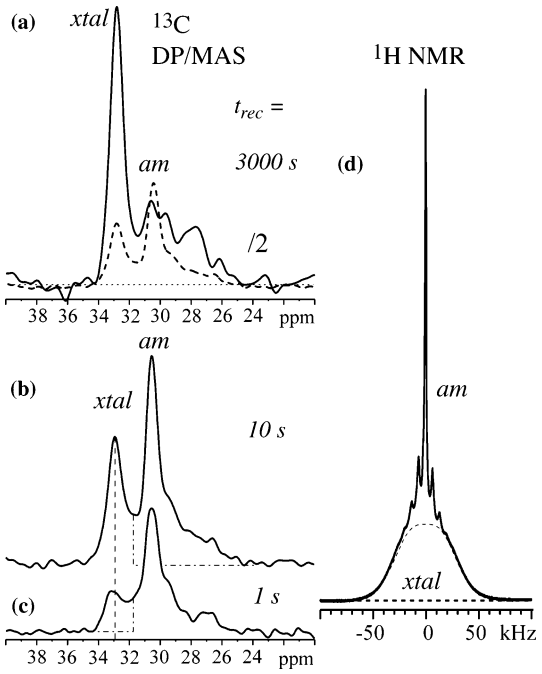

Figure 3. ^{13}C and ^1H NMR crystallinity determination. (a−c) DP/MAS ^{13}C NMR with recycle delays of (a) 3000 s (full line) and 10 s (dashed line), both shown on a per-scan basis and scaled down by a factor of 2. The signals at 28 ppm are due to segments near the ester groups. (b, c) Spectra with (b) 10 s and (c) 1 s recycle delays shown at full scale. Vertical and horizontal dash-dotted lines demarcate the spectral areas of the noncrystalline components (gauche-containing in (b), mobile all-trans in (c)). (d) ^1H wide-line spectrum acquired at 6.5 kHz MAS. The amorphous component shows four spinning sidebands, in addition to the centerband.

it is clearly observed in DP/MAS spectra with short recycle delays <10 s (Figure 3b). Given the methylene crystallinity of ca. 70% and the 75% fraction of regular $[-CH_2-]_n$ sites, the amorphous $[-CH_2-]_n$ peak makes up only $0.30 \times 0.75 = 23\%$ of the total $^{13}CH_2$ signal in quantitative ^{13}C NMR spectra. In

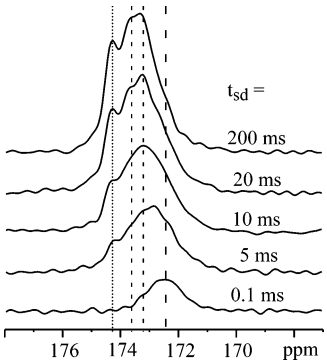

Figure 4. COO spectra after ^{1}H T_2 selection of 15 μs duration and ^{1}H spin diffusion of the durations indicated on the right, starting from the mobile amorphous regions.

CP spectra, the cross-polarization efficiency and consequently the signal of these noncrystalline segments are reduced due to the relatively high segmental mobility in the amorphous regions.

The series of DP/MAS ^{13}C NMR spectra in Figure 3 permits determination of the crystallinity.[5] Torchia CP/$T_{1,C}$ experiments show that the longest recycle delay of 3000 s provides a 93% relaxed crystalline signal intensity in the DP/MAS spectrum. The crystalline signal dominates the 3000 s DP/MAS spectrum, while the spectra with short recycle delays and more scans (Figure 3b,c) enable deconvolution of the amorphous signals. The heteronuclear nuclear Overhauser effect (NOE) has been suppressed by a 10 s delay before ^{13}C saturation pulses and the nominal recycle delay.[5]

^{1}H Wide-Line Spectrum. The ^{1}H spectrum of PE22,4 is shown in Figure 3d. As a result of static dipolar couplings, rigid segments will show broad ^{1}H lines, while these couplings will be partially averaged out by fast large-amplitude segmental motions, and the ^{1}H line width will be reduced.[17] On that basis, the ratio of protons in the mobile noncrystalline to that in the more rigid crystalline regions can be estimated. The small area fraction of the mobile segments of the spectrum in Figure 3d confirms the high crystallinity deduced from SAXS and ^{13}C NMR. The integral under the dashed line, which is an estimate of the crystalline fraction, is 70% of the total area. The uncertainty due the uncertain delineation between amorphous and crystalline regions is $\pm$7%.

^{1}H Spin Diffusion. Information on domain sizes and on the morphological location of specific functional groups with resolved resonances can be obtained from ^{1}H spin diffusion with ^{13}C detection. The greatly enhanced signal of the ^{13}C-labeled ester groups enables us to localize them with respect to the amorphous and crystalline phases. The technique measures diffusion of ^{1}H nuclear magnetization, which arises due to internuclear ^{1}H$-^1$H dipole$-$dipole interactions between domains of a solid polymer. In the Goldman$-$Shen experiment, ^{1}H magnetization in the mobile amorphous regions can be selected exclusively through a $T_{2,H}$ filter, which dephases the magnetization in the more rigid crystalline and interfacial regions.[14] After flipping the remaining magnetization of the mobile segments back to the *z*-direction, its ^{1}H spin diffusion through the intermediate interfacial regions into the crystallites can be observed after ^{13}C cross-polarization.[5,26]

After an initial short spin-diffusion time of 100 μs, only the upfield signal from carbonyl groups located in the amorphous regions can be observed (see the bottom trace in Figure 4). At intermediate spin-diffusion times, an increase in ^{13}COO signal intensity and a downfield shift of the main carbonyl signal to 173 ppm are seen, indicating spin diffusion into segments located at the amorphous$-$crystalline interface. At times >10 ms, relatively distinct resonancea near 174 ppm can be observed, apparently due to carbonyl segments buried inside the polyester crystals.

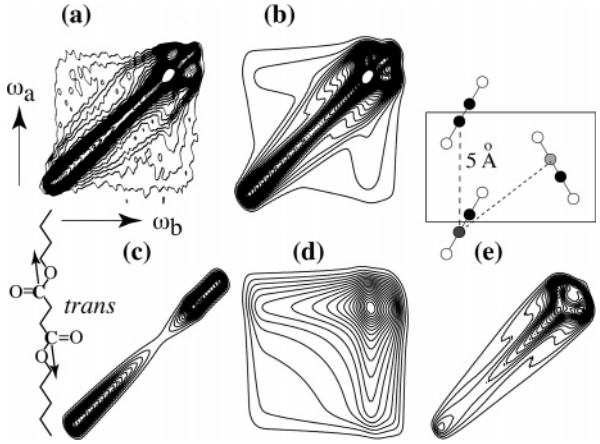

Figure 5. DOQSY NMR spectrum of 100% doubly ^{13}COO-labeled PE22,4. (a) Experimental spectrum. (b) Simulation based on three components: (c) intrasegmental correlation in all-trans chains in the crystallites, (d) random relative orientations in the noncrystalline regions, and (e) interchain correlations in the crystallites.

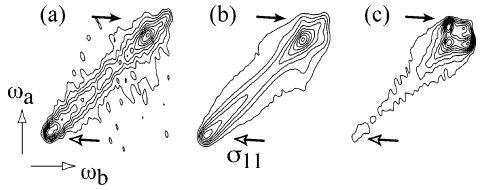

Figure 6. DOQSY NMR spectra of three differently ^{13}COO-labeled PE22,4 samples, processed and plotted comparably. (a) 16% doubly ^{13}COO-labeled, showing intensity mostly along the diagonal, as expected for correlations within an all-trans segment. (b) 100% doubly ^{13}COO-labeled (same data as in Figure 5a, but broadened and plotted like the spectrum in (a). (c) 100% singly ^{13}COO-labeled, showing only interchain correlations. Arrows mark characteristic differences between the intensity patterns.

DOQSY ^{13}C NMR Spectra. Figure 5 displays the sheared DOQSY spectrum of 100% doubly ^{13}C-labeled PE22,4. It exhibits three discernible spectral patterns: (i) a straight ridge on the diagonal, (ii) intensity near the diagonal that tapers at the left end of the spectrum (σ_{11}), and (iii) a low, broad pattern spread over a wide range of the spectral plane. In the following discussions of these features, correlations of ester groups within the same succinic acid moiety will be called intramolecular/intrachain, while correlations arising from neighboring ester groups are referred to as intermolecular/interchain. Note, however, that this convenient nomenclature is not strictly speaking accurate, since ester groups in neighboring chain stems in the crystal, which are termed intermolecular here, can be part of the same polymer chain.

In order to confirm this decomposition of the DOQSY spectrum into the three patterns convincingly and assign them, we have recorded DOQSY spectra of samples with different ^{13}C-labeling patterns. In a sample with the ^{13}C$-^{13}$C-labeled PE22,4 diluted to a fraction of 1/6 in unlabeled polymer, interchain correlation patterns will be suppressed to ca. 1/6. The spectrum of this sample (Figure 6a) is dominated by the straight ridge on the diagonal that is characteristic of the intramolecular correlation for an all-trans conformation. In order to make the comparison meaningful, the spectrum of the 100% doubly ^{13}C-labeled PE22,4, shown in Figure 5a, is replotted in Figure 6b with the same line broadening and the same contour levels relative to the largest peak in the spectrum. It still shows

significantly more off-diagonal intensity than the spectrum in Figure 6a, likely due to the interchain correlations.

These interchain correlations can be observed selectively in a PE22,4 sample with a single ^{13}C label per repeat unit. This results in a large distance of at least 28 Å to the next ^{13}COO group along the chain, so that medium-range intermolecular correlations can be observed selectively. The clear DOQSY pattern observed proves close interchain distances and can be used to elucidate the chain packing in the unit cell. In comparing with the intensity in (b), note that the signal in (c) is spread out in the 2D plane and that the single-^{13}COO labeling reduces the ^{13}C concentration 2-fold. Details of the chain-packing analysis are discussed below.

Chemical Shift Tensor Orientation. In order to be able to use the ^{13}C CSA of the ester groups as a reliable orientational probe, we need to know the ^{13}C chemical shift tensor orientation with respect to the chemical bonds. Generally, the tensor orientation of COO groups has been found to reflect the invariance of the local electron distribution under a reflection with respect to the ester plane, i.e., the plane containing the four atoms of the C−(C═O)−O moiety. The corresponding invariance of the chemical shift can only be achieved if a principal axis of the chemical shift tensor is perpendicular to the ester plane. In almost all esters studied to date, this axis is associated with the σ_{33} principal value. Given that a PE-like all-trans chain has the same symmetry, this symmetry principle is expected to apply to a good approximation to the esters in our sample. For measuring the relative orientation of the normals of the two inequivalent chains in the unit cell, the orientation of the σ_{33} chemical shift principal axis is particularly important.

In order to confirm this aspect of the tensor orientation experimentally, we have measured it by correlating the ^{13}C chemical shift anisotropy with the H−H dipolar coupling. In an all-trans structure, the H−H vectors connecting geminal protons are perpendicular to the ester plane. The HH/CSA experiment therefore measures the components of the chemical shift tensor perpendicular to the plane of the chain with particular sensitivity. The H−H distances and couplings indicated in Figure 7a show that within a given chain the geminal H−H dipolar coupling is an order of magnitude stronger than the other H−H interactions of the methylene protons nearest to the ester group. Therefore, the spectral pattern will be dominated by the geminal coupling, with more or less uniform line broadening from the large number of weaker intersegmental H−H couplings. The spectrum has little or no sensitivity to the small angle between the σ_{11} axis and the chain axis.

The preceding discussion of the tensor orientation and the structure shown in (a) assumes that the bond between the COO carbon and the neighboring CH_2 group is 180° trans. Fortunately, a rigorous analysis of the intermolecular DOQSY data can still be performed without such an assumption. The intramolecular part of the DOQSY spectrum in Figure 5 proves the four carbons of the succinate moiety to be in one plane, and both geminal H−H internuclear vectors are perpendicular to this plane. Thus, the HH/CSA experiment measures the orientation of σ_{33} with respect to the succinate C−C−C−C plane, and the DOQSY spectrum of singly ^{13}COO labeled PE22,4 reflects the angle between these planes in neighboring molecules.

The HH/CSA correlation experiment is quite simple; we have previously applied it to confirm the tensor orientation of methylene carbons.[27] Without sample rotation, an undecoupled ^{1}H dipolar evolution (t_1) is followed by relatively short Lee−Goldburg cross-polarization to ^{13}C, which prevents long-range C−H or H−H transfers. The ^{13}C chemical shift frequency is detected during t_2 under standard proton decoupling.

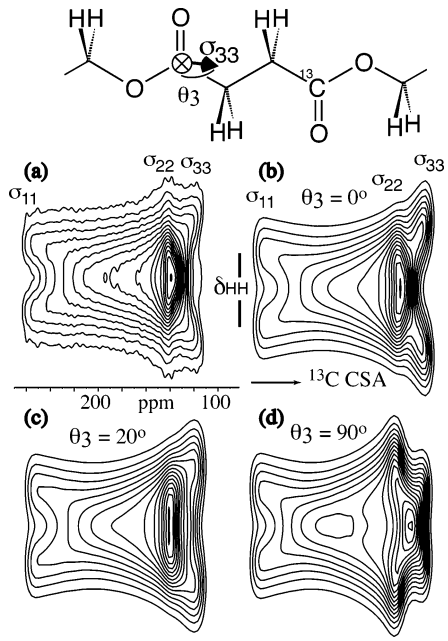

Figure 7. HH/CSA correlation for determining the ^{13}COO chemical shift tensor orientation in the crystallites of PE22,4, by correlation of ^{13}C CSA with the ^{1}H−^{1}H dipolar coupling in neighboring CH_2 groups. The relevant diester segment and the chemical shift tensor are indicated at the top of the figure. (a) Experimental spectrum. ^{1}H spin diffusion during CP has been suppressed by employing magic-angle-spin-lock (Lee−Goldburg) cross-polarization. (b) Best-fit simulated spectrum with the canonical tensor orientation that reflects the reflection symmetry with respect to the ester plane, for a trans conformation. (c) Simulated spectrum for a chemical shift tensor whose σ_{33} axis makes an angle of $\theta_3 = 20°$ with the normal to the ester plane. (d) Simulated spectrum with the orientation of the σ_{22} and σ_{33} axes interchanged relative to (a).

The resulting spectrum is shown in Figure 7a and compared with three simulations for different chemical shift tensor orientations. In Figure 8, the effects of the H−H dipolar modulation[28] during t_1 on the ^{13}COO spectrum in ω_2 are shown. This is an alternative way of displaying the information in this experiment. It is less affected by the "T_2 decay" resulting from the multiple long-range H−H couplings. The large splitting in Figure 8 and strong dipolar modulation near σ_{33} in Figure 7b show unambiguously that the σ_{33} axis is close to parallel to the H−H internuclear vector, i.e., normal to the plane of the chain. Comparison with the simulated spectra in Figures 7 and 8 confirms the canonical tensor orientation that reflects the local symmetry with respect to the O−C═O plane and excludes a ∼20° deviation of the σ_{33} axis from the chain normal.

Relaxation Time Measurements. The ^{1}H $T_{1\rho}$ values of the crystalline regions of PE22,4 and PE(32/12),4 were measured with ^{13}C detection after 1 ms of regular CP at various temperatures. They are shown in Figure 9 and compared to linear low-density polyethylene with an average crystallite thickness of ∼7 nm. The relaxation time $T_{1\rho}$ of ^{1}H magnetization spin-locked along a B_1 field in the rotating frame reflects motions with motional rates between $\sim 10^3$ and 10^7/s and exhibits a minimum for motional rates $k = \gamma B_1 = 300\,000$/s. In the polyesters studied here, a strong slowdown of relaxation is observed compared to that in the more random PE(32/12),4 and in a linear low-density polyethylene (see Figure 9).

The longitudinal ($T_{1,C}$) ^{13}C relaxation was measured using the sensitive Torchia method with a phase-cycled *z*-storage after CP.[15] Compared to saturation or inversion recovery, this method

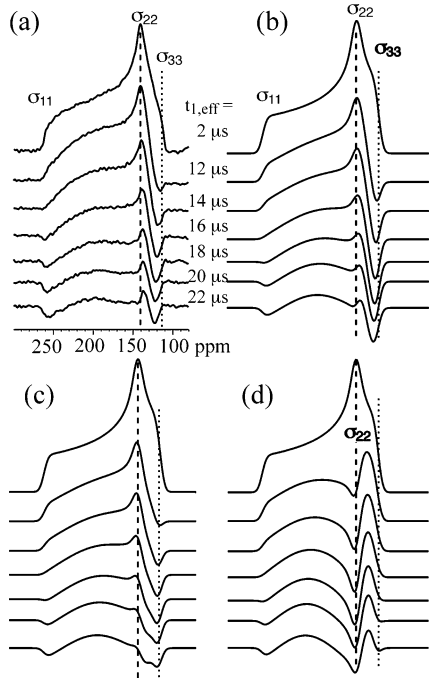

Figure 8. H−H dipolar modulated ^{13}C spectra, obtained after 0.2 ms of LGCP, using the same pulse sequence as for the 2D spectrum of Figure 7. (a) Experimental. (b) Best-fit spectra with the canonical tensor orientation in an all-trans structure. (c) Spectra for a chemical shift tensor whose σ_{33} axis makes an angle of 20° with the normal to the ester (or strictly speaking succinate) plane (compare Figure 7c). (d) σ_{22} perpendicular to the succinate plane (cf. Figure 7d).

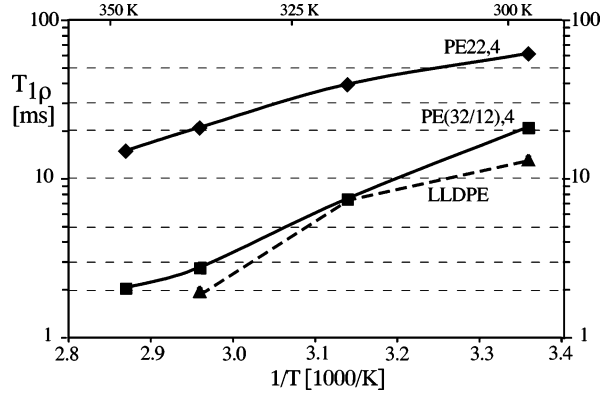

Figure 9. Arrhenius plot of the temperature dependence of ^1H $T_{1\rho}$ of crystalline regions for PE22,4, PE(32/12),4, and a quenched linear low-density polyethylene (LLDPE) of ca. 7 nm crystallite thickness.

also has the great advantage of a well-defined final magnetization value of zero. Figure 10 shows $T_{1,C}$ data for PE22,4 and PE(32,12),4, measured at two different temperatures. The curvature in this semilogarithmic plot proves significant non-exponentiality of relaxation, as also found in polyethylenes.[29] The apparently straight final portion for PE22,4 evaluated as described by Axelson et al.[29] has a $T_{1,C} \geq 700$ s. Again, a strong slowdown in the $T_{1,C}$ relaxation of PE22,4 compared with PE-(32/12),4 and literature data for polyethylene of similar crystallite thickness is observed.

Discussion

Crystallinity. The crystallinity is a crucial parameter in the structural characterization of semicrystalline polymers. It is obtained quite directly from quantitative ^{13}C and ^1H NMR, with conformation-dependent chemical shifts and motional narrowing, respectively, enabling identification of crystalline and

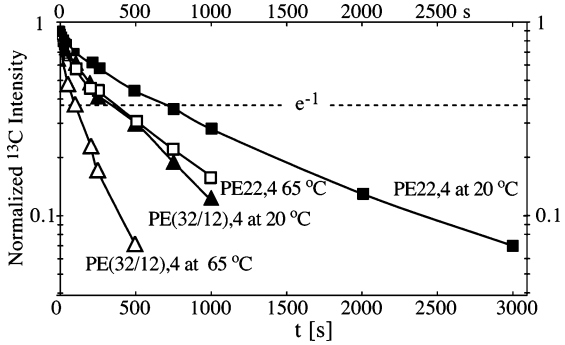

Figure 10. $T_{1,C}$ relaxation curves of CH_2 signals of PE22,4 (squares) and PE(32/12),4 (triangles) at 20 °C (filled symbols) and 65 °C (open symbols).

noncrystalline components. It can also be deduced from a detailed analysis of SAXS correlation functions or direct simulations of the SAXS diffractogram. While SAXS yields a volume crystallinity, $f_{c,V}$, NMR measures the relative number of segments in crystalline and amorphous regions, which gives the slightly larger mass-based crystallinity, $f_{c,m}$. The two quantities are related through the ratio of the crystal and sample densities, ρ_c/ρ_{sample}, by

$$f_{c,m} = f_{c,V}\rho_c/\rho_{sample} \quad (2)$$

In NMR, quantitative direct-polarization ^{13}C spectroscopy with long and short recycle delays (see Figure 3) yields a good estimate of the crystallinity in polyethylenes and related semicrystalline polymers.[5] After the short recycle delays (Figure 3b,c), the main peak of the amorphous fraction is clearly observed at 30.5 ppm. It is relatively narrow compared to the amorphous peak in polyethylene of similar crystallinity at the same temperature, indicating relatively high and uniform mobility. The signal is seen to rise with the recycle delay up to 10 s; a further rise is excluded on the basis of the match with the 3000 s spectrum. The small 33 ppm band observed in the 1 s spectrum appears to be distinct from the crystal peak, in terms of peak position, width, and relaxation time, and is therefore considered as part of the noncrystalline components. It accounts for 5% of all segments. As reported above, the DP/MAS spectrum with 3000 s recycle delay provides a 93% relaxed crystalline signal intensity, essentially yielding a quantitative peak area for the fully relaxed polymer. The 7% missing crystalline intensity is easily taken into account in the quantitative analysis. The area of the short-T_1 peaks at 30.5 and 33 ppm relative to that of the fully relaxed signal yields the fraction of amorphous methylene groups. Its complement, with a value of 70%, is the crystallinity of the methylene segments. This matches the value estimated from the ^1H spectrum in Figure 3d.

Since most of the ester groups are within the crystallites, the true crystallinity is somewhat higher. The $T_{1,C}$ relaxation behavior of the ester groups is different from that of the methylenes; therefore, we need to assess the fraction of crystalline and amorphous COO groups separately. The spectrum after CP from the mobile protons is seen at the bottom of Figure 4 after a 0.1 ms spin diffusion time. It accounts for 19% of the equilibrated spectrum at the top. In the 0.1 ms spectrum, the intensity is enhanced by $1/f_{amorphous} = 3$-fold since the ^1H magnetization is concentrated in the amorphous regions, while it spreads out over the whole repeat unit after longer spin diffusion. Thus, this signal accounts for 6.3% of COO groups. It allows us to calculate a corrected mass-based crystallinity of

$f_{c,m} = (0.7 \times 24 + 0.94 \times 6.6)/30.6 = 0.75$. This converts to $f_{c,V} = 0.72$ using eq 2 with density estimates based on polyethylene values, with the two C=O oxygens per 28 backbone atoms factored in, $\rho_c = 1.07$ g/cm^3 and $\rho_a = 0.92$ g/cm^3. Note that an inaccuracy of a few percent in the densities has only a minimal effect on the ρ_c/ρ_{sample} conversion factor.

The crystallinity in the direct simulation of the SAXS diffractogram (see Figure 1d,e) is $f_{c,V} = 0.75$. It is slightly higher than the number from NMR, possibly due to defects that are not included in the SAXS model of infinitely wide crystalline lamellae. An uncertainty of similar magnitude, ±2%, arises from the partial disorder at the amorphous−crystalline interface discussed below.

Crystallite Thickness and Diester Layering. SAXS shows that the long period is 77 Å, which, given a crystallinity of about 73%, results in a crystallite thickness of about 56 Å. Given that this exceeds the 34 Å length of the 28-backbone atom repeat unit of the polyester, such a crystal thickness can only be achieved by incorporation of ester groups deep into the crystal.

More conclusive evidence regarding this point can be gained by an examination of the correlation functions obtained from the SAXS patterns (Figure 1c). Correlation between diester planes appear prominently in the correlation function $\gamma_1(r)$ computed from the complete SAXS intensity data (top curve in Figure 1c) and in the correlation function computed from the (00*l*) layer lines only (bottom curve in Figure 1c). Three strong correlation peaks (excluding the one located at the origin, which results from self-correlation) can be detected in these curves.

Because the thickness of amorphous interlayers is quite close to the distance between diester planes in the crystals, it is a priori difficult to separate the scattering into intra- and intercrystallite contributions. However, the almost complete disappearance of correlation peaks for distances longer than the long period indicates that the correlation between the locations of diester planes in neighboring crystals is weak, except for distances strictly corresponding to the long period. This intercrystalline correlation appears as the last marked peak in the complete $\gamma_1(r)$ curve, for distances corresponding to the repeat period of the lamellar stacking, which can be obtained from the correlation function computed from the first SAXS peak only (middle curve in Figure 1c). Therefore, the peaks that are found in $\gamma_1(r)$ at distances shorter than the long period must by necessity originate predominantly from correlation between diester planes in the same crystals. As there are three such peaks (counting now the self-correlation peak centered at the origin), each crystal must include three diester layers.

The crystallite thickness is ~10% larger than twice the repeat period between diester planes, since that repeat period contains only two diester layers. With a repeat period of 27 Å calculated from the positions of the intense (00*l*) reflections in the SAXS diffractogram, the crystallite thickness is 59 Å.

NMR confirms that a crystal contains three diester layers, of which one is at the center of the crystallite, while the other two are at the interface to the amorphous layer. If only two diester layers were included in a crystalline lamella, at least 1/3 of the ^{13}COO groups would be found in the mobile loops that make up the amorphous regions. The ^{13}COO chemical shift powder pattern of Figure 1d, the spin diffusion data of Figure 4, and the 2D spectrum of Figure 7 show no indication of such a major highly mobile component. The strong intensity of the crystalline COO components in the DOQSY spectrum indicates that the interfacial ester groups are predominantly incorporated into the crystal lattice.

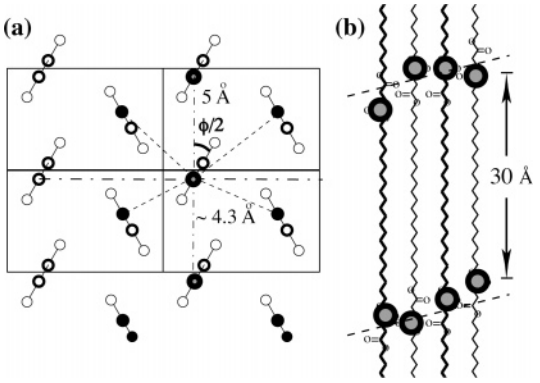

Figure 11. (a) Schematic representation of the crystal structure perpendicular to the chain axes, indicating the definition of the angle ϕ, as well as intermolecular distances. Note the parallel neighboring chains in the crystal, which produce intensity along the diagonal of a DOQSY spectrum. (b) Schematic representation of the large ^{13}C−^{13}C intramolecular distance in singly ^{13}COO-labeled PE22,4.

With 2/3 of ester groups at the surface and 1/3 in the center of the crystal, the necessity of an unambiguous distinction between inter- and intrachain correlations in DOQSY NMR is highlighted. The various diagonal and near-diagonal patterns in the fully labeled polymer (see Figure 5a) might be due to two different types of intramolecular correlations at the surface and center of the crystal. Using the singly ^{13}COO-labeled sample, we have selected the interchain correlation signal unambiguously and have shown that the elliptical pattern near the diagonal is due to strong intermolecular correlations, not an intramolecular correlation of esters at the crystallite surface.

The layering of the esters in the crystallites is reflected in the DOQSY NMR spectra. The interchain COO−COO distances within a diester layer are sufficiently close (Figure 11a) to produce significant ^{13}C−^{13}C double quantum coherences and corresponding DOQSY intensity. As a result, the spectrum of the singly ^{13}COO labeled PE22,4 (Figure 6c) shows strong DOQSY intensity, in spite of the lack of a ^{13}COO correlation partner nearby in the same chain. In this sample, ^{13}C labels along a given chain in the crystallites are separated by at least 28 Å (see Figure 11b), and the corresponding ^{13}C−^{13}C dipolar coupling is less than 1 Hz. Therefore, intrachain double-quantum coherences are completely negligible in the DOQSY spectra. The observed strong intermolecular correlation signal confirms that ^{13}COO groups in neighboring chains are preferentially close, rather than randomly distributed along the chains within the crystal.

Distribution of Interfacial Esters between Crystalline and Amorphous Regions. The SAXS and NMR analysis has shown that 2/3 of the diester layers are located at the crystallite surfaces. Of each of these ester double layers, only one individual layer of COO groups is located directly at the crystalline−amorphous interface; these interfacial COO layers thus contain 1/3 of all COO groups. The extent to which they are ordered can be assessed semiquantitatively by NMR. The fully amorphous ester component, contributing the upfield shoulder to the ^{13}C NMR spectrum of Figure 4, accounts for 6.3% of the COO groups (see above). In the spectra of Figure 4, there are indications of a second noncrystalline band slightly more downfield, centered near 173 ppm. Its location close to the interface is deduced from its fast polarization by spin diffusion from the amorphous regions. The intensity fraction of this partially disordered interfacial component is estimated at roughly 15%.

The DOQSY simulations with the crystalline packing parameters provide good fits of the patterns of both the singly

and the doubly labeled samples; this indicates that the majority of ester groups, including many at the interface, are in a crystalline environment. Nevertheless, the DOQSY spectrum of Figure 5a also shows a significant disordered fraction, with an integral intensity estimated at 30%. This component may be overrepresented in the DOQSY spectrum, since all conformations of the "diacid" segments have $^{13}C-^{13}C$ distances smaller than or equal to that in the all-trans conformation of the crystal. Thus, the $1/r_{CC}^3$ distance factor of double-quantum excitation is least favorable for the conformation in the crystal. In addition, if one COO group is in the amorphous region, and its partner is in the crystal, the DOQSY signal of both groups will appear disordered. Thus, the disordered interfacial esters account for ca. $(30\% - 7\%)/2 = 11\%$ of all COO groups. This corresponds to $\sim 11\%/33\% = 1/3$ of the COO groups directly bordering the amorphous regions.

Chain Conformation. The wide-angle X-ray diffractogram shows sharp and intense reflections signaling a dense orthorhombic crystal packing of the alkane segments. It demonstrates that PE22,4 packs laterally like short-chain alkanes with a predominantly planar zigzag conformation along the backbone. This agrees with the simplest interpretation of the DOQSY NMR spectrum of doubly ^{13}COO-labeled PE22,4 (Figure 5a), where the straight diagonal ridge can be assigned to segments along the same chain in all-trans conformation. This implies an intramolecular origin of the diagonal ridge, which is confirmed by its appearance in the spectrum of a 16% doubly ^{13}COO-labeled PE22,4, where the dilution has reduced the probability of ^{13}C-labeled neighboring chains 6-fold (see Figure 6a).

Strictly speaking, the diagonal ridge in the DOQSY spectrum does not require three trans bonds between the ester groups but only specifies that the ester group orientations are related by exact inversion symmetry. Nevertheless, this still results in a specific structural requirement because inversion symmetry can be achieved only if the central bond (OOC−C−C−COO) is 180° trans. The torsion angles of the other two bonds must have identical magnitude and opposite signs; this includes all-trans with +180° and −180°. Note that the central 180° trans conformation also fixes the $^{13}C-^{13}C$ internuclear distances to 3.9 Å and the angle between the $^{13}C-^{13}C$ internuclear vector and the local chain axis to 15°. In addition, it requires that the H−H internuclear vectors of the two succinate CH_2 groups are exactly parallel to each other and perpendicular to the C−C−C−C plane of the succinate moiety; this is relevant for the ^{13}COO CSA tensor orientation measurement by correlation with the H−H dipolar couplings.

The intensity distribution along the diagonal ridges of Figure 6a,b shows a distinct modulation by the $^{13}C-^{13}C$ dipolar coupling. In particular, the left, $\sigma_{11} = 262$ ppm, end of the spectrum exhibits a significantly enhanced intensity compared to the powder pattern in Figure 2d. This indicates that this direction corresponds to the strongest $^{13}C-^{13}C$ dipolar coupling. In other words, the σ_{11} axis of the chemical shift principal-axes system is approximately along the $^{13}C-^{13}C$ internuclear vector, which is tilted from the chain axis by only ~15°.

Chain Packing in the *a,b*-Plane. The orthorhombic packing of the alkane segments deduced from WAXD is confirmed by observation of the infrared Davydov splitting characteristic of orthorhombic crystals such as polyethylene or linear alkanes, which is compatible with both O⊥ and O′⊥ subcells.[30] However, as nonzero l $(hkl)_s$ reflections in WAXD are weak and not well-separated from the dominant $(hk0)_s$ reflections, it is not possible to decide from WAXD whether O⊥ or O′⊥ packing is adopted.

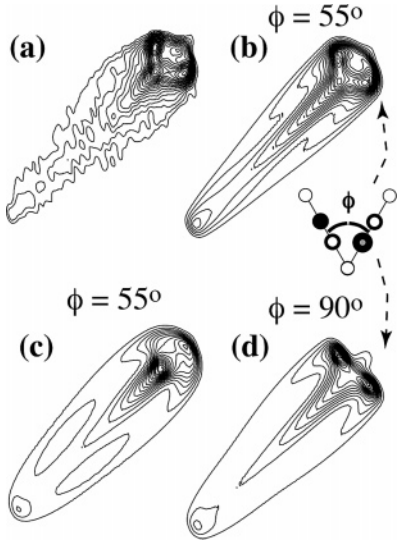

Figure 12. DOQSY spectrum of singly ^{13}COO-labeled PE22,4. (a) Experimental spectrum (same data as in Figure 6c). (b) Simulation for an O′⊥ crystal modification with a 55° angle between ester planes, for the structure sketched in Figure 13a. (c) Simulation for the closely related structure sketched in Figure 13b, for the same 55° angle between ester planes. (d) Simulation for the O⊥ crystal modification, with a 90° angle between ester planes.

NMR can shed further light on the chain packing. As discussed above, the "boat-shaped" DOQSY intensity pattern in the singly ^{13}COO-labeled PE22,4 (Figure 12a) must be attributed exclusively to interchain correlations. The good signal strength and specific spectral pattern provide reliable information on the interchain ester distances and the relative orientation of the ester planes, as indicated in Figure 11a. The intermolecular signal is quite strong because there are four relatively close neighboring chains with nonparallel planes, containing eight ester groups, compared to only one ester carbon nearby along the same chain.

The experimental DOQSY pattern for the singly ^{13}COO-labeled sample (Figure 12a) consists of two main contributions: (i) an off-diagonal pattern that is most prominent in the upper right-hand corner of the spectrum and must be due to correlations between nonequivalent chains, and (ii) a diagonal ridge that must arise from correlations between parallel chains in neighboring units cells. The intensity distribution of the off-diagonal pattern reflects the relative orientation of the ester groups. The observed absence of significant off-diagonal intensity near the σ_{11} (lower left) end of the spectrum is expected: This principal value corresponds to a direction close to the chain axis, and the chain axes in the crystal are all parallel. Therefore, the frequencies ω_A and ω_B in this spectral region will be similar, i.e., close to the diagonal.

The most reliable and nontrivial quantity derived from this spectrum is the angle between the normals of the ester planes of the two nonequivalent chains in the unit cell. This measurement requires knowledge of the orientation of the ^{13}COO chemical shift tensor with respect to the chemical bonds. As described above, correlation with the H−H internuclear vector in the nearby CH_2 groups confirms that here, as in almost all other ester groups studied to date, the σ_{33} principal axis is along the normal to the plane of the ester group.

Figure 12b shows a best-fit simulation with an angle of $\phi = 55°$ between the planes of nonequivalent chains. The six nearest-neighbor chains in the crystal structure have been included in the simulation, using the double-quantum spin-pair approximation, which is appropriate for these weak dipolar couplings. The

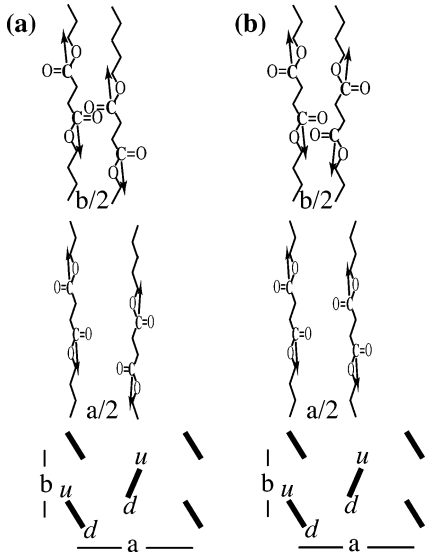

Figure 13. Schematic representation of different ester-group orientations in the O⊥′ structure. Projections onto the *bc*, *ac*, and *ab* planes are shown (from top to bottom). The labels "u" and "d" in the *ab*-plane projection indicate "up" and "down" pointing units. Without ester units, the two structures would be identical. They are related by a displacement (and 180° rotation) of the ester units by one CH_2 unit. The DOQSY NMR data of Figure 12 strongly favor the structure in (a).

angle of 55° deviates significantly from that in the orthorhombic unit cell of polyethylene, where the planes of the chains are essentially perpendicular, i.e., $\phi = 90°$. Spectra simulated with this angle show a straight ridge perpendicular to the main diagonal near the upper right-hand corner of the spectrum (see Figure 12d). This is clearly different from the elliptical broadening observed in the experimental spectrum.

While the "shape" of the diagonal ridge in the spectra of Figure 12 is prescribed by the identical orientation of corresponding chains in different unit cells and does not provide new geometric information, the intensity distribution along the diagonal reflects the angle between the plane of the chain and the C−C interchain vector connecting neighboring equivalent chains. This angle is directly related to the angle ϕ between the planes of neighboring chains discussed above. The intensity modulation of the diagonal can resolve ambiguities that remain with the off-diagonal pattern from the inequivalent-chain correlation:

In a given chain, the ester group can take two different orientations. The transition from one to the other is achieved by a 180° rotation around the chain axis (and displacement by one CH_2 unit, if the rest of the chain structure should remain unchanged). Figure 13 displays two possible relative orientations of ester groups within the given O′⊥ sublattice. The CSA tensor orientation does not change strongly by this 180° rotation; in particular, the orientation of the σ_{33} principal axis is unchanged. Nevertheless, the orientation of the σ_{11} axis changes by at least 15° (actually 22° according to the tensor orientation found here), which is significant enough to result in distinct spectral patterns. The best-fit simulation of Figure 12b corresponds to the relative orientation shown in Figure 13a, while the structure in Figure 13b would produce the spectrum shown in Figure 12c, which is inconsistent with the experimental pattern. The simulations thus indicate that the ester groups in neighboring nonequivalent chains are closer to parallel, with smaller angles between the C−O bonds in the two nonequivalent chains. The off-diagonal signal intensity in the upper right corner of the simulations of Figure 12b,c is clearly different.

In summary, the angle between the planes of nonequivalent chains is found to be 55° ± 20°. The error margin includes residual uncertainties in the tensor orientation. This significant deviation from 90° is in favor of the O′⊥ crystal subcell structure.

Chain Tilt and Displacement. The 27 Å spacing of diester planes calculated from (00*l*) reflections in the SAXS diffractogram is smaller than the calculated extended length of 34 Å for one repeat unit. Assuming an all-trans planar zigzag conformation of the chains, this deviation must be attributed to a tilt angle of 37° of the chain axes relative to the normal of the layers of ester groups. The tilt with respect to the normal to the basal plane allows the chains to maintain the energetically favorable polyethylene-like crystal packing while keeping ester groups close to one another in a quantized gliding process.

In other words, ester groups on neighboring chains must be displaced relative to each other along the chain axis. The DOQSY NMR spectrum depends on the glide plane arrangement, since the length and direction of the $^{13}C-^{13}C$ internuclear vectors changes, and thus the dipolar modulation of the double-quantum spectrum. Nevertheless, among the large number of different displacement geometries there are several that provide acceptable fits, so a unique geometry cannot be identified. The fit provided by the simulation of Figure 12b shows that the experimental DOQSY NMR spectrum of Figure 12a is consistent with the SAXS-derived displacement. It assumed a displacement of the ester groups by *c* (i.e., two methylene units) along both the *a*- and *b*-axis, i.e., an $\alpha\beta_{22}$ glide plane. This means that each neighboring chain is displaced by $c = 2.54$ Å. Note that the relative intensity of the intrachain diagonal ridge and the crystalline off-diagonal interchain correlation pattern in the DOQSY spectrum is not a free parameter but is determined by the internuclear distances in the crystal structure. Because of the presence of two ester groups separated by 3.9 Å in each repeat unit, even with displacements on the order of 3 Å along neighboring chains, at least two out of the four ester groups in a pair of neighboring chains will be spatially close and thus produce significant intensity in the DOQSY spectrum.

Detailed Structural Model. Figure 14 summarizes many of the specific structural features deduced from the SAXS and NMR data. The good quality and consistency of the data, combined with the high regularity and long repeat unit of the polymer, permit the analysis to extend almost seamlessly from segmental (0.3 nm) to morphological (10 nm) length scales. On the basis of the measured crystallinity, the crystallite thickness, and the chain tilt relative to the crystal surface, all of which are indicated in Figure 14, we can determine the average number of repeat units in the amorphous and crystalline phases. Typically, two $(CH_2)_{22}$ and three $OOCC_2H_4COO$ units, with the expected all-trans conformation, form a crystalline stem, while the $(CH_2)_{22}$ portion of a third repeat unit produces a highly mobile loop in the amorphous region.

The ester groups form three diester layers in the crystallite: one in the center and two at the crystalline−amorphous interfaces. The majority, but not all, of the interfacial ester groups exhibit crystalline conformational and packing order, according to DOQSY NMR. The figure also highlights that due to the completely regular spacing of the COO groups along the chain, the details of one diester layer are reproduced exactly in neighboring diester layers in the same crystallite. Two smaller-scale features determined by DOQSY NMR but not displayed in Figure 14 are the 55° angle between the ester planes of the two chains in the unit cell and the relative orientation of the C═O bonds, as shown in Figures 11a and 13a.

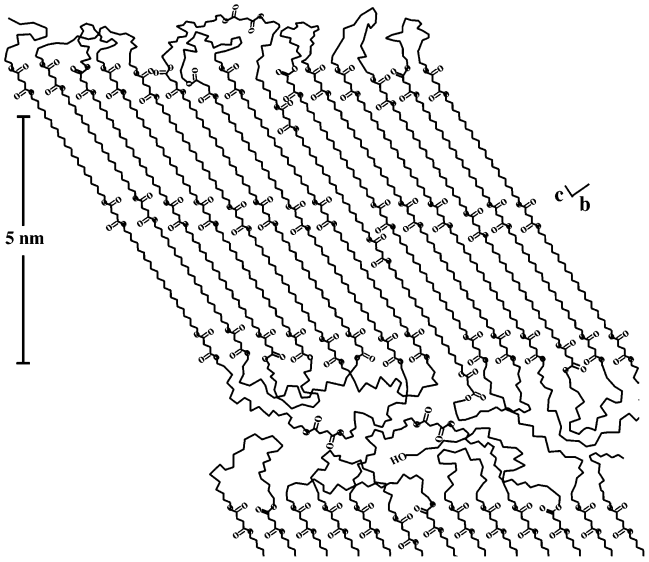

Figure 14. Molecular and supramolecular structure of the PE22,4 aliphatic polyester according to SAXS and NMR. It consists of 5.6 nm thick crystallites, 2 nm thick amorphous layer made up mostly of $(-CH_2-)_{22}$ chain loops, a diester layer in the center of the crystallite, and a partially disordered diester layer at each crystallite surface. Occasional displaced chains in the crystallite, as suggested by $T_{1\rho}$ relaxation, are also indicated.

Chain Folding. Given the level of details on the morphology of this specific semicrystalline polymer, it becomes possible to estimate the relative proportion of loose loops and tie molecules at the crystal surface, a still controversial issue between the proponents of regular folding and the supporters of a more disordered model of the crystalline−amorphous interface.[31] As shown in Figure 14, the 6.3% amorphous ester moieties by necessity belong to long loops between distant stems of the same crystal or to tie molecules bridging two neighboring crystals. This provides an upper bound for the fraction of long loops and tie molecules vs tighter C_{22} folds.

Accordingly, out of 1000 diester moieties, 63 belong to long loops and tie molecules while 937 belong to crystals. The 937 crystalline diester groups correspond to 937/3 = 312 crystalline stems. These are terminated either by a chain end, by a relatively tight C_{22} fold, or by a longer loose loop or tie molecule. Given a polymer molar mass of 14 100 g/mol, a stem molar mass of 964 g/mol (Figure 14) and a "molar" crystallinity of ∼0.75, there are 14100/(964/0.75) = ∼11 stems per polymer chain. These are connected by 10 folds or tie molecules and terminated by two chain ends. Therefore, out of the 624 ends of the 312 crystalline stems, 57 are terminated by a chain end (9%), 2 × 63 = 126 are connected to a loose loop or tie molecule (20%), and the remaining 441 are connected to a tighter C_{22} fold (71%).

Chain Flips in the Crystallites. Scattering and NMR have provided a detailed view of the structural features of PE22,4. Ester layering is one of the most striking features. Its effect on the chain dynamics, especially in comparison with polyethylene, can be assessed by relaxation time measurements. In polyethylenes, the chains have been shown to undergo 180° flips coupled with displacements by one methylene unit.[6,32] Depending on the crystallite thickness, the jump rate at ambient temperature is 1 − 1000/s, and it increases steeply with increasing temperature and decreasing crystallite thickness.[33−35] This motion drives ^1H $T_{1\rho}$ relaxation of spin-locked magnetization, which provides information on the motion of CH_2 groups in the 10−1000 kHz region.[6] The chain dynamics also affect the T_{1C} relaxation: As a result of many individual jumps, chain diffusion occurs between crystalline and amorphous regions, and ^{13}C magnetization is transported from the fast-relaxing amorphous regions into the crystallites.[32] This process can explain the strong crystallite thickness and temperature dependence of $T_{1,C}$ relaxation in polyethylenes.[29] Vibrations in the crystallites on the nanosecond time scale would produce a weaker or even opposite temperature dependence.

The relaxation data in Figures 9 and 10 demonstrate that although the ester functionalities account for only about 15% of sample mass, they slow down the dynamics compared to that in polyethylene. While the polyethylene exhibits fast $T_{1\rho}$ relaxation driven by the 180° chain flips, the relaxation is slowed down ∼10-fold in PE22,4, even though it has a smaller crystallite thickness. The slowdown of the dynamics can be attributed to the layering of the ester groups, which either restricts the chain motion to occasional localized flip-flops without translation or requires cooperative motions of a chain bundle in the crystallites. This interpretation is confirmed by the fast relaxation in polyester PE(32/12),4, which has the same fraction of esters as PE22,4 but with the layering of esters disrupted by the random variations in the oligomethylene segment length.

The reduction in ^1H $T_{1\rho}$ with increasing temperature (see Figure 9) indicates that even in PE22,4 some chain motion still occurs. It can be speculated that at any given time a small fraction of ester groups are out of register. This would permit the corresponding chains to undergo fast flips, until the ester groups are moved back into register.

The $T_{1,C}$ relaxation curves of the crystalline CH_2 signals of PE22,4 and PE(32/12),4 at two temperatures are shown in Figure 10. Again, the relaxation in PE22,4, with a 700 s "final" relaxation time at 20 °C, is much slower than in PE(32/12),4 and also than in PE with a crystallite thicknesses of <6 nm, where the long-time $T_{1,C}$ is <50 s.[29] The strong slowdown of the relaxation in PE22,4 supports our conclusion that chain flips are suppressed by the ester−ester interactions.

Conclusions

State-of-the-art solid-state NMR and SAXS data of an aliphatic polyester with widely but regularly spaced ester groups provide a detailed picture of the molecular and 10 nm morphological structure. The results show that ester groups exert a measurable influence on the crystal structure as well as the crystal thickness and the tilt angle between chain axes, while still allowing crystallization in a polyethylene-like crystal lattice. DOQSY NMR confirms the all-trans structure of the succinate unit between the ester groups. In a singly ^{13}COO-labeled sample, DOQSY NMR proves intermolecular correlations due to the layering of ester groups detected by SAXS. The NMR intensity pattern observed reflects the relative orientation of neighboring chains with a 55° angle between the planes of the chains. The ^{13}COO chemical shift tensor orientation has been confirmed by correlation with the geminal H−H dipolar coupling of neighboring CH_2 groups. The 73 ± 3% crystallinity determined from quantitative ^{13}C NMR and SAXS, together with the 7.7 nm long period from SAXS, requires that typically two crystalline repeat units of a given chain alternate with a noncrystalline loop consisting of one $(-CH_2-)_{22}$ unit. The C_{22} loops connect ca. 71% of the ends of crystalline stems, while 9% are terminated by chain ends and 20% are connected to a loose loop or tie molecule. Both SAXS and NMR show convincing evidence of three diester layers in the crystal, of which two are at the surfaces and one is in the center of the crystal.

Measurements of relaxation times $T_{1\rho}$ and $T_{1,C}$ confirmed that, in spite of the relatively small fraction of ester groups along

the poly(methylene) chains, fast 180° chain flips as observed in polyethylene are strongly suppressed in PE22,4. Comparison with linear low-density polyethylene of comparable crystal thickness and with PE(32/12),4, which introduces randomness into the ester placement, revealed that layering of ester groups cooperatively controls the dynamics of the chains in the crystallites.

Apart from providing very detailed structural information on a specific polyester containing long alkane segments, our study also shows that a few ester groups, regularly introduced into an otherwise purely aliphatic polymer, are sufficient to control the morphology of a polyethylene-like polymer to some extent. Strong intermolecular H-bonds such as found in polyamides are thus not essential to force quantization of crystal thickness and length of folds. This may be of some interest for chemists attempting to control the structure of interphase and amorphous regions (tight folds, loose loops, tie molecules, etc.) in semicrystalline polymers.

Acknowledgment. This work was supported by the NSF Materials Research Science and Engineering Center (MRSEC), DMR-9809365, at the University of Massachusetts. The use of MRSEC shared facilities is gratefully acknowledged. M. Gabriele Menges thanks 3M, Honeywell, and Reliance corporations for financial support through the Center for UMass/Industry research on Polymers (CUMIRP) at the University of Massachusetts.

References and Notes

(1) Ehrenstein, M.; Sikorski, P.; Atkins, E.; Smith, P. *J. Polym. Sci., Polym. Phys. Ed.* **2002**, *40*, 2685−2692.
(2) Le Fevere de Ten Hove, C.; Penelle, J.; Ivanov, D. A.; Jonas, A. M. *Nat. Mater.* **2004**, *3*, 33−37.
(3) Menges, M. G.; Schmidt-Rohr, K.; Penelle, J. *Abstr. Pap. Am. Chem. Soc. Polym.* **2002**, *224*, 573.
(4) Schmidt-Rohr, K. *Macromolecules* **1996**, *29*, 3975−3981.
(5) Hu, W.-G.; Schmidt-Rohr, K. *Polymer* **2000**, *41*, 2979−2987.
(6) Hu, W.-G.; Boeffel, C.; Schmidt-Rohr, K. *Macromolecules* **1999**, *32*, 1611−1619.
(7) Hu, W.-G.; Schmidt-Rohr, K. *Acta Polym.* **1999**, *50*, 271−285.
(8) Rusanova, E. E.; Sebyakin, Y. L.; Volkova, L. V.; Evstigneeva, R. P. *Zh. Org. Khim.* **1984**, *20*, 279−282.
(9) Hünig, S.; Buysch, H. *Chem. Ber.* **1967**, *100*, 4010.
(10) Kobayashi, H.; Nakamura, N. *Cryst. Res. Technol.* **1995**, *30*, 495−500.
(11) Holmes, D. L.; Lightner, D. A. *Tetrahedron* **1996**, *52*, 5319−5338.
(12) Brown, R. D.; Godfrey, P. D.; Elmes, P. S.; Rodler, M.; Tack, L. M. *J. Am. Chem. Soc.* **1985**, *107*, 4112−4115.
(13) Bennett, A. E.; Rienstra, C. M.; Auger, M.; Lakshmi, K. V.; Griffin, R. G. *J. Chem. Phys.* **1995**, *103*, 6951−6958.
(14) Goldman, M.; Shen, L. *Phys. Rev.* **1966**, *144*, 321.
(15) Torchia, D. A. *J. Magn. Reson.* **1978**, *30*, 613.
(16) Schmidt-Rohr, K. *J. Magn. Reson.* **1998**, *131*, 209−217.
(17) Schmidt-Rohr, K.; Spiess, H. W. *Multidimensional Solid-State NMR and Polymers;* Academic Press: London, 1994; Vol. 478.
(18) Abrahamson, S.; Dahlén, B.; Löfgren, H.; Pascher, I. *Progress in the Chemistry of Fats and Other Lipids;* Pergamon: London, 1978; Vol. 16, p 125.
(19) Abrahamson, S. S.-S. S.; Stenhagen, E. *Progress in the Chemistry of Fats and Other Lipids*; Pergamon: London, 1963; Vol. 7, p 1.
(20) Segerman, E. *Acta Crystallogr.* **1965**, *19*, 789.
(21) Vand, V. *Acta Crystallogr.* **1951**, *4*, 104.
(22) Small, D. M. *Handbook of Lipid Research;* Plenum Press: New York, 1986; Vol. 4.
(23) Fuller, C. S.; Frosch, C. J. *J. Am. Chem. Soc.* **1939**, *61*, 2575.
(24) Le Fevere de Ten Hove, C. Controlling Solid-State Microstructure of Semi-Crystalline Polymers through Chemical Design of Chains: a Study of Model Polyesters. Ph.D. Université Catholique de Louvain, Louvain-la-Neuve, 2001.
(25) Schmidt-Rohr, K. *J. Appl. Crystallogr.* **2007**, *40*, 16−25.
(26) Eckman, R. R.; Henrichs, P. M.; Peacock, A. J. *Macromolecules* **1997**, *30*, 2474−2481.
(27) Dunbar, M. G.; Sandström, D.; Schmidt-Rohr, K. *Macromolecules* **2000**, *33*, 6017−6022.
(28) Hartzell, C. J.; Pratum, T. K.; Drobny, G. *J. Chem. Phys.* **1987**, *87*, 4324−4331.
(29) Axelson, D. E.; Mandelkern, L.; Popli, R.; Mathieu, P. *J. Polym. Sci., Polym. Phys. Ed.* **1983**, *21*, 2319−2335.
(30) Koenig, J. L. *Spectroscopy of Polymers;* American Chemical Society: Washington, DC, 1992.
(31) Ivanov, D. A.; Pop, T.; Yoon, D. Y.; Jonas, A. M. *Macromolecules* **2002**, *35*, 9813−9818.
(32) Schmidt-Rohr, K.; Spiess, H. W. *Macromolecules* **1991**, *24*, 5288−5293.
(33) Mansfield, M.; Boyd, R. H. *J. Polym. Sci., Polym. Phys. Ed.* **1978**, *16*, 1227−1252.
(34) Boyd, R. H. *Polymer* **1985**, *26*, 1123−1133.
(35) Boyd, R. H. *Polymer* **1985**, *26*, 323−347.

MA071590P